Legless Locomotion: A Novel Locomotion Technique for Legged Robots

Ravi Balasubramanian
Computer Science and Engineering,
University of Washington,
Box 352350,
Seattle, WA 98195-2350, USA
bravi@cs.washington.edu

Alfred A. Rizzi
Boston Dynamics,
614 Massachusetts Avenue,
Cambridge, MA 02139, USA

Matthew T. Mason
Robotics Institute,
Carnegie Mellon University,
5000 Forbes Avenue,
Pittsburgh, PA 15213-3890, USA

Abstract

We present a novel locomotion strategy called legless locomotion *that allows a round-bodied legged robot to locomote approximately when it is high-centered. Typically, a high-centered robot is stuck since the robot's legs do not touch the ground. Legless locomotion uses the legs as a reaction mass to set up oscillatory body rotations which when coupled with ground contact gradually translate the robot. Legless locomotion's continuous dynamics differs from previously studied locomotion methods because of the simultaneous interaction of gravity-induced oscillations, a configuration-dependent system inertia, and non-holonomic contact constraints. This paper employs simple models to capture the complex dynamics and uses the intuition developed from the models to develop gaits that provide planar accessibility. We also present a quantification of legless locomotion's properties using simulations and motion-capture experiments.*

KEY WORDS—legged robots, mobility, dynamics and kinematics.

1. Introduction

This paper explores the mobility available to a high-centered legged robot—a robot whose legs cannot touch the ground. Our interest in the problem arose from experiments with a hexapod robot in uneven terrain. The robot, RHex (Saranli et al. 2001) (see Figure 1), has a simple design where each singly actuated compliant leg can rotate around its "hip". While this design, inspired by a cockroach, offers significant mobility, RHex can be easily trapped when it becomes high-centered, as there is no contact between its legs and the ground. The only possible means of locomotion when the robot becomes high-centered is to use the dynamic effect of swinging the legs, where the legs act simply as a reaction mass (see Extension 1). However, the question of how the robot should swing its legs to induce translation remains. While random flailing may induce incremental translation, the robot's motion tends to be hard to predict and control.

In at least one case, it is interesting to note that the high-centered RHex can move even when only being able to generate small forces. Suppose that RHex's body is rounded and the obstacle is flat; then, there is a single rolling contact between RHex's body and the obstacle. In this configuration, even small torques can cause the robot's attitude to oscillate, and these oscillations can interact with the body-obstacle rolling contact to produce translation. This paper shows that a high-centered robot has complete planar accessibility (meaning it can locomote anywhere in the plane) by rocking and rolling on its body using leg-swing motions. We call such a locomotion mode *legless locomotion*. Legless locomotion is not a general alternative to conventional legged locomotion, because it is typically slow and inefficient. Furthermore, the translation induced by legless locomotion is difficult to predict precisely,

The International Journal of Robotics Research
Vol. 27, No. 5, May 2008, pp. 575–594
DOI: 10.1177/0278364908091023

Figures 1–21 appear in color online: http://ijr.sagepub.com

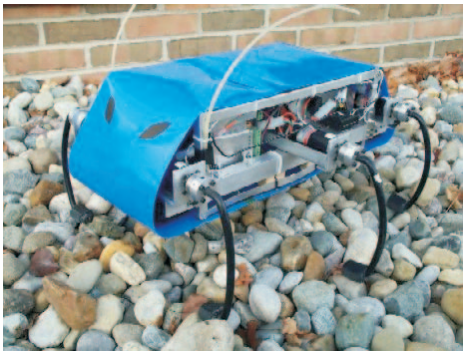

Fig. 1. The RHex experimental platform (http://rhex.net).

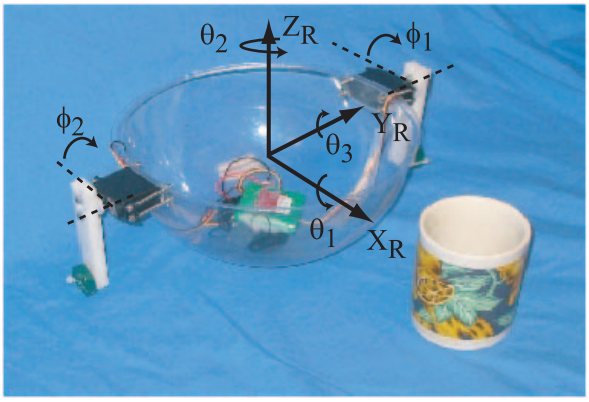

Fig. 2. The RRRobot experimental platform uses halteres to induce body-attitude oscillations leading to body translations.

because modeling contact between a rounded body and the ground is complex. However, even the approximate mobility that legless locomotion provides is useful in the special situation where a robot is high-centered and its conventional locomotion mode is infeasible. The overarching principle is that having a choice of locomotion modes for different circumstances ultimately contributes to robust mobility. Legless locomotion's dynamics differs from previously studied systems, as it is dynamic, continuous, oscillatory, and exploits the interaction between a variable system inertia and non-holonomic contact constraints in the presence of gravity. This paper provides an analysis of legless locomotion and develops suitable gaits.

For our experiments we built a special prototype robot called *The Rocking and Rolling Robot* (*RRRobot*, see Figure 2). RRRobot is a hemisphere with two actuated legs which can never touch the ground—it is permanently high-centered. Since RRRobot's legs act only as reaction masses, they are better called *halteres*, after the dumbbells sometimes used by athletes to give impetus in leaping.

Ignoring RRRobot's leg motions for a moment and focusing only on RRRobot's spherical contact with the ground, Figure 3 shows a sequence of interleaved pitch and yaw body rotations that induce RRRobot to translate. A challenge in legless locomotion is to find the leg motions that create such body-attitude oscillations which, when coupled with the non-holonomic slip-free contact constraints, cause RRRobot to locomote in the plane. The goal being to significantly outperform random leg motions which may induce essentially random incremental translation, this paper explores a low-dimensional gait space for legless locomotion that enables systematic travel.

Our experiments and simulations with RRRobot suggest that body-attitude oscillations produced by leg motions are a practical, albeit imprecise, way of translating a high-centered robot (see Figure 4 for an example gait). Furthermore, legless locomotion offers a new perspective on dynamically coupled locomotion, in particular the simultaneous interaction between a configuration-dependent inertia, the oscillatory dynamics, and the contact kinematics.

To the best of our knowledge, our work is the first to find gaits for a dynamic, oscillatory, continuous locomotion mode that exploits the simultaneous interaction of shape changes, a varying inertia, and non-holonomic contact constraints in the presence of gravity. After a brief review of related work in Section 2, we present the legless locomotion dynamics models in Section 3. We present legless locomotion gaits in Section 4 with results from experiment and simulation. We emphasize that the models we use provide insight into the legless locomotion's structural quality, rather than an exact quantitative reproduction of the robot's performance in the experiment. Portions of this paper have appeared in Balasubramanian et al. (2003, 2004).

2. Related Work

We now review background and related work, organized into three sections:

- Locomotion techniques.
- Locomotion error and recovery.
- Techniques for modeling mechanical systems.

2.1. Locomotion Techniques

Legged locomotion, which involves discontinuous contact, has been studied for the mobility it offers (McMahon 1984; Raibert 1986; McGeer 1990; Full and Tu 1991; Bares and Wettergreen 1999; Zeglin 1999; Linnemann et al. 2001; Saranli et al. 2001; Sakagami et al. 2002; Nagasaka et al. 2004). Similarly, wheeled locomotion, which involves continuous rolling, has

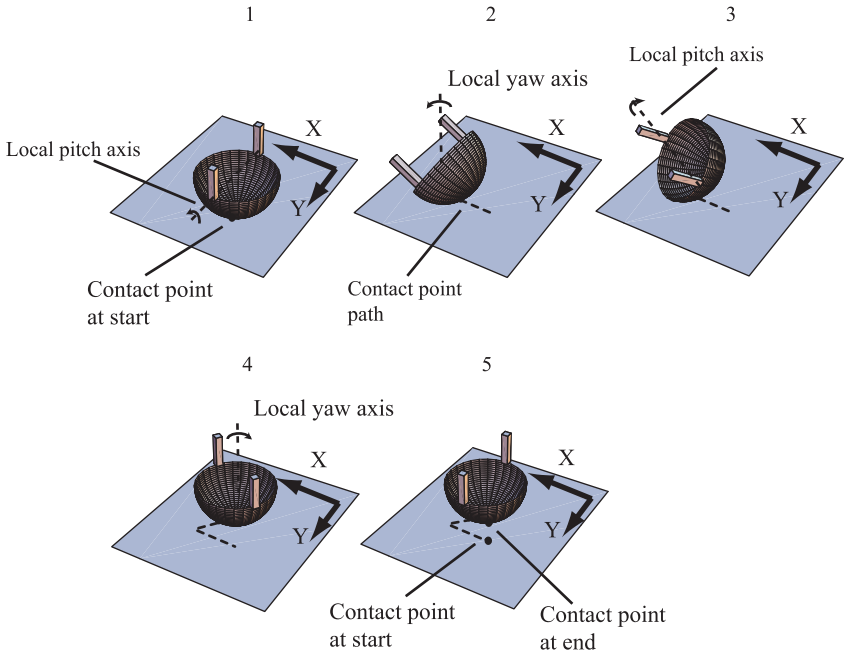

Fig. 3. Body pitch–yaw rotations that produce locomotion. Motions are represented as rotations about axes attached to the body. There is a local pitch rotation between positions 1 and 2 and positions 3 and 4; there is a local yaw rotation between positions 2 and 3 and positions 4 and 5.

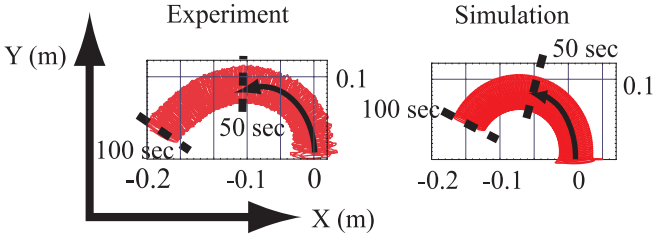

Fig. 4. A legless locomotion gait: counter-clockwise translation produced by roll–pitch–yaw body oscillations resulting from sinusoidal leg motions (Balasubramanian et al. 2004).

been explored for the efficiency it offers in a structured terrain (Reeds and Shepp 1990; Bellaiche et al. 1991; Sussmann and Tang 1991; Luca and Risler 1994; Jean 1996; Ostrowski 1996; Laumond 1998; Endo et al. 1999). Undulatory or snake-like locomotion offers stability and traction (Dowling 1997), and many interesting aspects of undulatory locomotion (in the absence of gravity) have been explored by using the snakeboard (Lewis et al. 1994; Ostrowski 1996; Bullo and Lewis 2003) and roller racer (Krishnaprasad and Tsakiris 1998) as prototypes. Several adaptive locomotion modes such as rolling, "slinky", and caterpillar-like locomotion have been suggested for modular robots (Yamawaki et al. 1994; Yim 1994; Lee and Sanderson 2002). Similarly, novel reconfigurable robot platforms have been designed to enable climbing, rolling, and walking (Phipps and Minor 2005; Shores and Minor 2005). Finally, the robotic locomotion problem has been considered as the dual of the manipulation problem, since the goal in both problems is to move a robot with respect to an object. Relevant to this paper, several researchers have explored, using kinematic models of motion, the motion of a sphere on a plate (Mukherjee et al. 2002; Das and Mukherjee 2006) or between plates (Bicchi and Marigo 2002).

Legless locomotion, the locomotion mode we propose for locomoting high-centered robots, has a combination of properties that differentiates it from previously studied locomotion modes. Legless locomotion's continuous dynamics differentiates it from usual walking, running, climbing, and jumping gaits, where contact between foot and the ground is intermittent. Legless locomotion's oscillatory dynamics differentiates it from continuous and kinematic or quasistatic rolling locomotion. Also, most undulatory locomotion techniques studied so far operate in the absence of gravity. In summary, legless locomotion is an underactuated, dynamic, oscillatory, and continuous locomotion mode that maintains a rolling contact between its body and the ground. In addition, legless locomotion exploits a configuration-dependent inertia, and its passive dynamics is induced by gravity. Legless locomotion's interesting features resulting from the interplay of contact constraints and body rotational dynamics are explored in detail in Section 3 of this paper.

2.2. Mobile Robot Error Recovery

Our legless locomotion work began as a recovery strategy for a high-centered robot. Leveraging previous studies of error recovery is difficult, since how a mobile robot fails and how it recovers depend directly on the specifics of its design, the environment, and uncertainty in the dynamics. Carlson and Murphy (2005) present a survey of how unmanned ground vehicles fail, using data from various urban search-and-rescue operations. While stating that mobile-robot reliability was low, they list actuators and the control system as two primary failure causes.

Most prior work on error diagnosis focuses on using high-level reasoning techniques on sensor data (Verma et al. 2003) and not on how robots become stuck. However, there is prior research in finding robot maneuvers that could act as error recovery techniques, although they are not portrayed as error recovery techniques. Hale et al. (2000) present a singly actuated hopping robot that reorients itself before propulsion. Once the robot lands, it reorients itself in the required direction of translation. Tunstel (1999) discusses a genetic programming approach to finding uprighting maneuvers for a nanorover. The algorithm evaluates the maneuver quality using the power consumed, the time elapsed, and the percentage of progress made.

While recovery modes allow a robot to return to its stock locomotion mode, some robot designs allow conventional locomotion modes to function even after an error. For example, researchers at Carnegie Mellon have developed a highly maneuverable robot called Spinner[1] (Sofman et al. 2006) that has an actuated suspension and can operate even when inverted. Similarly, RHex, the six legged robot, can walk upside-down also, but uprighting is useful when RHex uses automatic vision to navigate. Saranli and Koditschek (2002) presents back-flips as a technique for "uprighting" RHex. Returning to the problem of locomotion for a high-centered RHex, there are at least four different contact phenomena that a high-centered legged robot can exploit to translate using leg-swing motions (see Figure 5):

1. If the robot has a curved bottom, then the body rotations can incrementally translate the robot assuming slip-free body–ground contact (rolling legless locomotion, see Figure 3 and Extension 2).
2. If the robot has an irregular bottom and the protrusions act as "feet", a series of rolling and yawing body motions translates the robot by shifting its weight from one "foot" to another (walking legless locomotion, similar to the Rotopod (Lyons and Pamnany 2005)).
3. If the robot has a flat bottom, a net translation force can be produced using jerky leg motions (sliding legless locomotion, similar to the Universal Planar Manipulator concept (Reznik and Canny 1998)).

1. See http://www.rec.ri.cmu.edu/projects/autonomous.

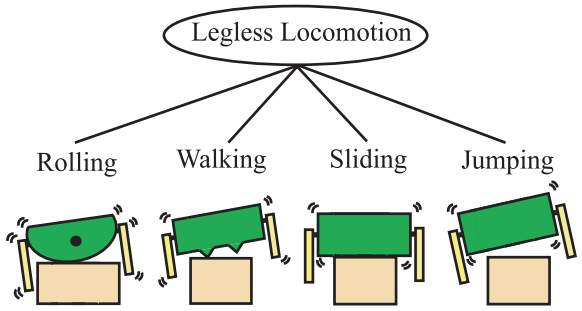

Fig. 5. Four types of legless locomotion: rolling, walking, sliding, and jumping.

4. If the robot's actuators have sufficient power and the leg-body mass ratio is sufficiently large, then the robot could move by rapidly swinging the legs and jumping (Berkemeier and Fearing 1998).

All four methods are potentially useful ideas for error recovery depending on the robot's design and circumstances. This paper focuses on the first strategy that uses pure rolling, because it offers a viable locomotion mode for a robot with inertial properties like RHex using small reaction forces. Henceforth, this paper will refer to rolling legless locomotion just as legless locomotion.

2.3. Dynamic Systems Modeling Techniques

Finding the dynamic and kinematic principles underlying a robot's motion is essential for developing appropriate control techniques. We now briefly review the various modeling techniques that have been used for different mobile robots.

Legless locomotion involves the interplay between body roll–pitch–yaw attitude dynamics and kinematic non-holonomic contact constraints. Numerous investigators have studied dynamic systems with constraints using Lagrangian dynamics (Craig 1989) or the energy-momentum method. Lewis et al. (1994) study the constrained mechanics of the constant-inertia *snakeboard* (see Figure 6), a modified version of a skateboard in which wheel directions can be controlled. The snakeboard rider locomotes by twisting his/her body back and forth, while simultaneously moving the wheel directions with a suitable phase relationship. Lewis et al. present numerical simulations of snakeboard locomotion using characteristic wheel motions and discuss a framework for studying mechanical systems with constraints in a coordinate-free form. Zenkov et al. (1997) discuss the energy–momentum method for control of dynamic systems with non-holonomic constraints such as the rattleback, the roller racer, and the rolling disk. After identifying system symmetries, Zenkov et al. use momentum equations to analyze the system. We use the Lagrangian method to study RRRobot's dynamics.

Fig. 6. The snakeboard (Lewis et al. 1994).

While RRRobot's body spatial position and orientation (called the *fiber space* (Bloch et al. 2003)) are not directly controlled, its leg configuration (called the *base space*) is controllable. Ostrowski (1996) presents a method for studying systems where the fiber space can be represented as a group. Since only the base space is actuated, Ostrowski finds a *connection* relating the base space velocities to the fiber velocities. Ostrowski's technique focuses on systems with constant inertias, simple constraints, and no gravity, such as the snakeboard and the Hirose snake. Shammas et al. (2007) go further to provide a unified approach to motion planning for dynamic underactuated mechanical systems with non-holonomic constraints. However, since RRRobot's motion is influenced by gravity, neither Ostrowski's nor Shammas's framework can be used directly to explore legless locomotion.

RRRobot locomotes by rolling its round body on the planar surface. The curvatures of the two surfaces and the type of contact between the two surfaces determine the kinematic constraints and, consequently, the relative motion between the two bodies. Montana (1988) derives the equations of motion for the contact point between two moving rigid bodies using differential geometry. Camicia et al. (2000) provide an analysis of the non-holonomic kinematics and dynamics of the *Sphericle* (Bicchi et al. 1997), a hollow ball driven on a planar surface by an unicycle placed inside. Bhattacharya and Agrawal (2000) present a spherical rolling robot that locomotes using two orthogonal rotors placed inside. They derive driftless equations of motion using the conservation of angular momentum and the contact constraints. The Sphericle, Bhattacharya's robot, and RRRobot have similar non-holonomic contact constraints, but RRRobot's oscillatory body rotations differentiates its planar motion (see Murray et al. (1994) and Li and Canny (1990) for more details on non-holonomic constraints). If we ignore RRRobot's ground contact constraints and assume RRRobot is floating in space, the problem of controlling RRRobot's body motion reduces to simply controlling its body attitude. This permits an analysis of the reaction forces between RRRobot's body and its legs without the environment's influence. Fernandes et al. (1994) discuss near-optimal non-holonomic motion planning for coupled bodies using Lagrangian dynamics and the principle of angular momentum conservation. Modeling a falling cat as two links attached either through an actuated universal joint or an actuated spherical joint, Fernandes et al. find plans to land a falling cat on its feet from an arbitrary starting point. RRRobot's body-attitude control problem is different because both the hip joints are aligned. This results in large reaction forces on the body pitch freedom, while the reaction forces are small on the body roll and yaw freedoms. Also, the roll and yaw body motions are induced by the non-linear effects that arise from a configuration-dependent inertia. It can be shown that by repeatedly wiggling the legs while exploiting the inertia variances, RRRobot can adjust its orientation. This contrasts with satellite reorientation using spinning reaction wheels—the inertias of the satellite system do not change with rotation of reaction wheels (Rui et al. 2000), and hence non-aligned reaction wheels are necessary for complete control.

2.4. Summary

Our work on the novel locomotion mode called legless locomotion is at the intersection of three areas: (1) dynamic systems modeling; (2) dynamic systems motion control and planning; and (3) mobile robotics. The above section touches some of the related work, while balancing between algorithmic techniques for mechanical systems and experimental mobile-robotics research. We emphasize that the problem we explore, namely the high-centered robot locomotion problem, has not been explored before and offers new insights into control for mechanical systems. We now present the models used to study legless locomotion.

3. Legless Locomotion Models

3.1. RRRobot's Dynamics

We begin studying *legless locomotion* by exploring the motion of RRRobot on a plane. The model is simple, consisting of a hemispherical shell with two short actuated legs hinged at revolute joints (see Figure 2). The massless shell has radius r, and the massless legs have length l. There are five masses on the robot: a reaction mass at the distal end of each leg (M_l), a servo mass where each leg is hinged (M_s), and the battery and processor mass at the bottom of the shell (M_b). Torques τ_1 and τ_2 may be applied at the leg joints, and the shell rolls on the plane without slip.

RRRobot's configuration q_{rr} consists of the sphere's position and orientation $(x, y, R(\theta_r, \theta_p, \theta_y))$ with respect to a spatial frame and the internal configuration of its legs (ϕ_1, ϕ_2). We choose to represent the orientation of RRRobot's shell using the roll–pitch–yaw fixed-angle convention (Craig 1989).

This representation defines any spatial orientation as a sequence of the following rotations: a roll rotation, followed by a pitch rotation, followed by a yaw rotation, all expressed in a frame aligned with the spatial frame. Note that there are several choices to represent orientation, but the dynamic properties are unaffected by the choice. Thus, RRRobot's configuration is given by

$$\begin{aligned} q_{rr} &= (x, y, R(\theta_r, \theta_p, \theta_y), \phi_1, \phi_2)^{\mathrm{T}} \\ &\in \mathbb{R}^2 \times SO(3) \times \mathbb{S}^1 \times \mathbb{S}^1. \end{aligned} \tag{1}$$

The equations of motion for RRRobot on a plane can be derived using Lagrangian dynamics (Craig 1989) and take the form

$$\begin{aligned} & M(q_{rr})\ddot{q_{rr}} + C(q_{rr}, \dot{q}_{rr})\dot{q}_{rr} + G(q_{rr}) \\ &= \tau + (\lambda_1 \omega^1)^{\mathrm{T}} + (\lambda_2 \omega^2)^{\mathrm{T}} + \zeta_{rr}, \end{aligned} \tag{2}$$

$$\omega^1 \dot{q}_{rr} = 0, \tag{3}$$

$$\omega^2 \dot{q}_{rr} = 0, \tag{4}$$

$$\omega^1 = (1, 0, -r\cos\theta_p \sin\theta_y, -r\cos\theta_y, 0, 0, 0), \tag{5}$$

$$\omega^2 = (0, 1, r\cos\theta_r \cos\theta_y, -r\sin\theta_y, 0, 0, 0), \tag{6}$$

where $M(q_{rr}) \in \mathbb{R}^{7\times7}$ represents the positive-definite non-diagonal configuration-dependent mass matrix, $C(q_{rr}, \dot{q}_{rr})\dot{q}_{rr} \in \mathbb{R}^7$ the vector of Coriolis and centrifugal terms, $G(q_{rr}) \in \mathbb{R}^7$ the vector of gravitational terms, $\zeta_{rr} \in \mathbb{R}^7$ the energy loss, and $\tau = (0, 0, 0, 0, 0, \tau_1, \tau_2)^{\mathrm{T}}$ the generalized force. The generalized force τ indicates that only the legs are actuated. The gravitational terms cause RRRobot to behave as a pendulum (for small-amplitude oscillations), and RRRobot's pitch and roll natural frequencies are governed by its mass distribution and the shell's curvature. Thus, when the legs are swung along oscillatory trajectories, the superimposition of the dynamic effect of leg swings, gravity, and contact losses cause RRRobot to behave as a forced damped oscillator (Jose and Saletan 1998). The sphere–plane no-slip contact constraints (Montana 1988) are defined by (3) and (4). The one-forms in (5) and (6) define the directions in configuration space along which the tangential contact forces act. The symbols $\lambda_1, \lambda_2 \in \mathbb{R}$ represent the magnitudes of the contact constraint forces. A detailed discussion of sphere–plane no-slip contact kinematics is available in Section 3.2. RRRobot loses energy when it rolls on the ground. For example, when RRRobot is released from a non-zero body pitch or roll configuration and is allowed to oscillate without leg swings, oscillation amplitude decreases with time, until the robot stops oscillating. Also, if RRRobot is spun about its contact point (that is, the robot yaws in the plane), the robot stops rotating after some time—again because the robot loses energy due to friction with the ground. However, these body–ground traction losses in legless locomotion are difficult to model, and this paper seeks simple models that provide an approximation of system behavior and remain tractable for use in planning. The energy loss that occurs when RRRobot rolls on the ground or spins about the contact point arises from a combination of dry and viscous friction. Dry friction results from body–ground slip, while viscous friction results from the body–ground rolling interaction as well as aerodynamic effects. Dry friction is easy to model using, say, a Coloumb friction model, but including Columbic loss makes RRRobot's dynamical model significantly more complex. The primary complication arises from RRRobot's dynamics becoming hybrid; that is, RRRobot's dynamics would then transition between two models depending on whether the traction forces exceed the friction cone—one model when the body slides on the ground (traction forces exceed the friction cone), and another when the body rolls on the ground (traction forces inside the friction cone). Since this research focuses on understanding RRRobot's novel coupled motion and not on modeling contact between two surfaces, we ignore dry friction in our simulations of RRRobot. This also implies that we do not model differences between static and dynamic friction. As a first approximation, we bundle all ground contact losses into a viscous damping term ζ_{rr}.

On the other hand, viscous damping losses can be included without resorting to a hybrid model. Detailed rolling resistance models are available in (Brilliantov and Poschel 1998) and (Poschel et al. 1999) and, in reality, RRRobot's viscous losses are possibly coupled across rotational axes. For example, the damping losses for translation are coupled with pitch and roll rotation damping losses, and yaw rotational losses are also possibly coupled with pitch and roll configuration. For simplicity, we model viscous losses simply as being proportional to configuration velocities along each axis. This paper does not present the detailed experiments required to glean the viscous-loss parameters and achieve a perfect match of RRRobot motion between simulation and experiment. We choose viscous damping coefficients ζ_{rr} that permit a qualitative comparison between RRRobot's motion in the experiment and the simulation. Needless to say, neglecting dry friction and approximating it with a simple viscous friction model introduces differences in robot path between simulation and experiment, as we will see in Section 4.1.

3.2. RRRobot's Sphere–plane Contact Kinematics

In this section, we study RRRobot's sphere–plane contact kinematics (Montana 1988) independent of the leg-body dynamics. The non-holonomic sphere–plane contact constraints given by (3) and (4) define the relationship between a sphere's roll–pitch–yaw velocities and its planar translation velocity. Thinking about a sphere rolling on a plane, we notice that if the robot pitches while roll and yaw are zero, the robot translates in the X direction. Similarly, if the robot rolls while pitch

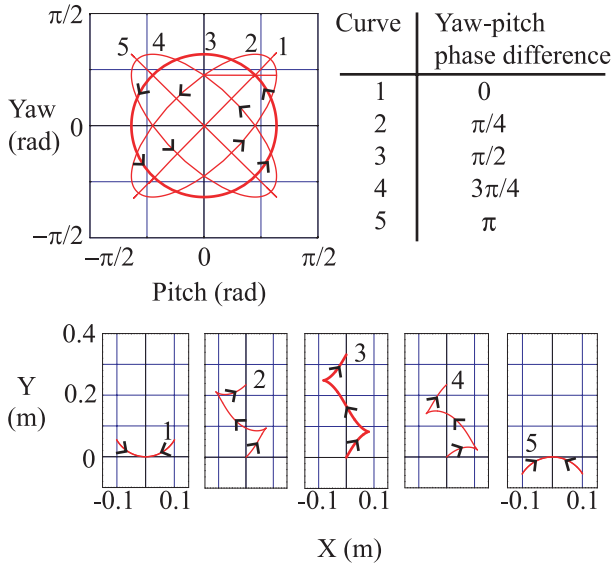

Fig. 7. The path taken by a sphere rolling on a plane changes with body-attitude trajectory. The contact point evolves over one cycle for different pitch–yaw phase relationships, given by $\theta_r = 0, \theta_p = \sin(t)$, and $\theta_y = \sin(t + \beta_y)$, where β_y is the yaw–pitch phase difference.

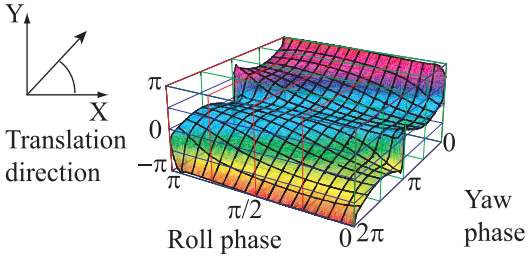

Fig. 8. Body-fixed translation direction for a sphere (radius 0.12 m) on a plane after one cycle in body-rotation space given by $\theta_r = \sin(t + \beta_r), \theta_p = \sin(t)$, and $\theta_y = \sin(t + \beta_y)$, where β_r is the roll-oscillation phase and β_y the yaw-oscillation phase relative to pitch oscillations.

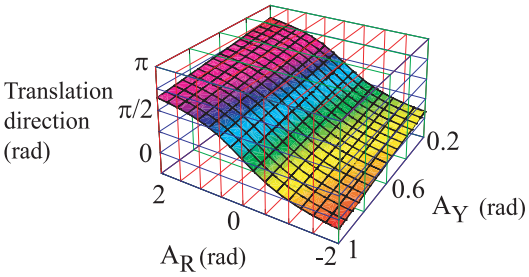

Fig. 9. Body-fixed translation direction for a sphere (radius 0.12 m) on a plane after one cycle in body-rotation space given by $\theta_r = A_r \sin(t + \pi/2), \theta_p = \sin(t)$, and $\theta_y = A_y \sin(t + \pi/4)$, where A_r is the roll oscillation amplitude and A_y the yaw oscillation amplitude.

and yaw are zero, the robot translates along the Y direction. If RRRobot's yaw orientation is, say, 45°, the robot's pitching motion causes it to roll along a line that is rotated 45° from the X-axis. Due to RRRobot's spherical body and our choice of configuration representation, yaw rotations produce zero translation of the sphere center (and the contact point which is directly below), even at non-zero pitch or roll configuration. This is because the yaw configuration velocity is expressed about an axis perpendicular to the plane, and accordingly, the fifth element in the one-forms in (5) and (6) is zero. Finally, note that elements 6 and 7 in ω^1 and ω^2 are zero, indicating that leg configuration does not contribute to the contact kinematics.

Li and Canny (1990) have shown that a ball on a plane is globally controllable; that is, the ball can roll from any configuration on the plane to another. We are interested in exploring how body rotational oscillations relate to net contact-point displacement. First, consider an example where roll is constant while pitch and yaw configuration are sinusoidal over time with unit amplitude. Figure 7 shows the net motions for various choices of the yaw–pitch phase difference. Note that net displacement along the global X-axis is zero for any choice of phase difference. If we choose roll–yaw oscillations (with zero pitch), net contact-point displacement is along the global X-axis. Note that attitude oscillation frequency only time scales the path. Now consider a more complicated motion where roll, pitch, and yaw configuration are all sinusoidal over time with unit amplitude, but pitch–yaw and pitch–roll phase differences are independently variable. Then translation in any direction is possible (see Figure 8 which shows net translation direction over one cycle (in the body-fixed frame) as a function of the two phase differences; also see Extension 3). Finally, we consider a motion where the phases are determined, but the roll and pitch amplitudes vary. Figure 9 shows how translation direction (in the body-fixed frame) varies with the choice of roll and pitch amplitude. Since RRRobot's legs are aligned with its body-fixed Y-axis, pitch oscillations tend to dominate over roll oscillations. So, RRRobot's predominant translation mode is along the body-fixed Y-axis.

Thus, from Figures 8 and 9, we notice that by varying the body-attitude phase and amplitude relationships, a sphere can *rock and roll* along any direction. An important point to note here is that translation direction is fixed for a given phase and amplitude relationship; that is, cyclic body-attitude oscillations produce net linear translation. So what body rotations can induce RRRobot's translation to curve? Consider the case where yaw configuration drifts over time in addition to the robot maintaining pitch–yaw or roll–yaw oscillations. Figure 10 provides an example of how translation curves when body yaw

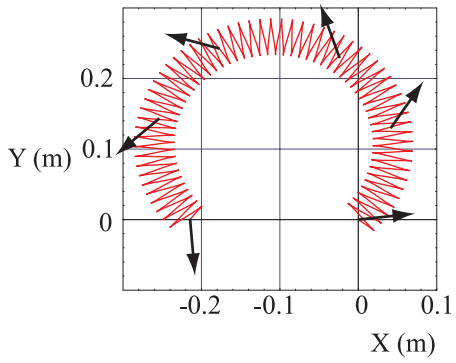

Fig. 10. Contact-point time history for a sphere (radius 0.12 m) on a plane starting from the origin for the body-rotation phase relationship given by $\theta_r = \theta_p = 0.15\sin(8t)$, and $\theta_y = 0.1t + 0.15\sin(8t + \pi/2)$. The arrows indicate the direction the robot faces (yaw orientation).

drifts linearly with time in addition to the sphere maintaining sinusoidal roll, pitch, and yaw oscillations—the robot moves in a circle while oscillating back and forth. In this example, the roll, pitch, and yaw oscillations have constant amplitude, phase, and frequency, and yaw drifts over time. If yaw does not drift, the robot moves in a straight line (similar to the cases in Figures 8 and 9). Translation curvature increases as yaw drift rate increases, and the path radius becomes smaller. In summary, linear translation arises from an appropriate (fixed) phase relationship between body-attitude oscillations. These oscillations when coupled with yaw drift (over time) result in curved translation. Note that while we use sinusoidal body rotations to illustrate the contact kinematics, RRRobot's body-attitude oscillations created by the leg motions are not necessarily sinusoidal. Also, even though the contact kinematics permit translation in any direction for different body-attitude trajectories, RRRobot's leg-body dynamics limits the range of locomotion. Similarly, the limited roll–pitch–yaw phase relationships produced by the leg dynamics limit translation velocities. However, curved translation is possible since we can produce varying body-yaw drift rates using leg trajectories that produce varying inertias (Balasubramanian et al. 2003).

Since we are specifically interested in RRRobot's net translation, we characterize RRRobot's translation speed and direction using its net motion over a body rotation cycle and not its instantaneous state. Thus, even if RRRobot's attitude oscillations cause it to deviate from its average path, we only use its net translation over a cycle to characterize its speed and direction. A challenge in legless locomotion is to find the leg motions that produce the body rotations to induce the desired translation. We now explore gaits for legless locomotion that allow full planar accessibility.

4. Legless Locomotion Gaits

One way to think about gaits for legless locomotion is to consider the body–ground contact kinematics and the leg-body dynamics separately. In the previous section, we explored kinematic coupling between the body and the support plane, while neglecting the dynamic effect of either the leg actuation or the floor contact on the body oscillations. We now consider just the interplay between the dynamics of RRRobot's leg motions and body rotations. First, we notice that RRRobot's swinging legs can produce a combination of pitch, roll, and yaw body rotations. These coupled rotations make the mapping between leg motions and body oscillations complex. Suppose for simplicity we imagine that RRRobot's leg motions create body rotations along each axis individually without any coupling (see Figure 11). Then, we can glean individual mappings, albeit approximate, between leg motions and yaw rotations (with the robot hinged at its body center), leg motions and pitch rotations, and leg motions and roll rotations. Such a mapping is simpler when compared with the mapping between leg motions and RRRobot's coupled body rotations.

Using the simplified pitch-dynamics model, we note that swinging the legs in-phase with each other creates pitch oscillations due to a combination of reaction forces and gravity. Using the simplified yaw-dynamics model, we note that swinging the legs 180° out of phase about the vertical configuration produces yaw oscillations due to reaction forces. Combining these two insights while keeping in mind that legless locomotion's dynamics is continuous, we notice that swinging the legs 90° out of phase with each other (half-way between completely out-of-phase and in-phase) about the vertical configuration produces both pitch and yaw oscillations simultaneously. Coupling this understanding with the sphere–plane contact kinematics, we note that appropriate leg trajectories can produce pitch–yaw oscillations, which in turn induce translation. Since we focus on gaits where the legs are close to the vertical configuration and RRRobot's leg axes are aligned with its body-fixed Y-axis, roll oscillations have small magnitude compared with pitch oscillations, and so do not contribute directly to RRRobot's translation.

So what leg motions induce yaw drift (or net yaw rotation) which is required for curved translation? For this, we will take a closer look at the simplified yaw dynamics model. It is apparent from the angular momentum conservation principle that the body yaws due to the reaction forces from leg swing motions. For example, if we move the left leg forward from the vertical-up configuration while keeping the other leg stationary, the body undergoes a positive yaw rotation. However, if the leg makes a complete rotation, the body returns to its start configuration.

An important property of the yaw model that we can use to produce net body yaw is its configuration-dependent inertia (Balasubramanian and Rizzi 2004; Balasubramanian 2006). Here is a simple thought experiment with the simplified yaw-

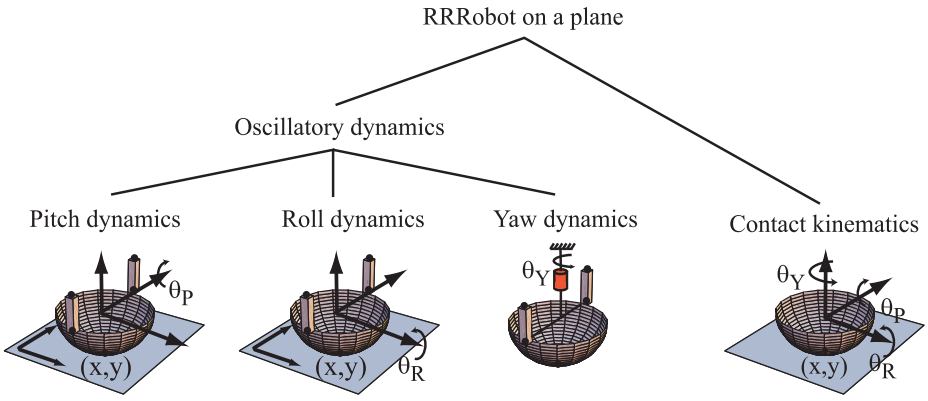

Fig. 11. Decoupled RRRobot dynamics.

Table 1. Incremental motion of the yaw model.

Time interval	$\phi_1(t)$	$\phi_2(t)$	Change in yaw
0–1	$0 \rightarrow \pi/2$	0	ϵ_1
1–2	$\pi/2$	$0 \rightarrow \pi/2$	$-\epsilon_2$
2–3	$\pi/2 \rightarrow 0$	$\pi/2$	$-\epsilon_2$
3–4	0	$\pi/2 \rightarrow 0$	ϵ_1
Net change in yaw			$2(\epsilon_1 - \epsilon_2)$

dynamics model. We will move each leg back and forth between extremes of 0 and $\pi/2$. Each leg will dwell at the extreme for 1 s and will take 1 s to transition between angles following a cubic spline. The result is a Lie bracket-inspired (Murray et al. 1994) smoothed square wave, with the two legs out-of-phase with each other. This sequence of leg motions yields a net yaw motion, as shown in Table 1 and can be confirmed by studying the table and thinking about the yaw angular inertia of the system. Suppose the body yaw is ϵ_1 during the interval $t = 0$ to $t = 1$, and is ϵ_2 during the interval $t = 1$ to $t = 2$. The net yaw during the two motion segments is different, because the yaw angular inertia varies depending on whether the leg is stretched out or tucked in. This difference produces net yaw at the end of the motion sequence. This same property of producing net yaw motion using yaw inertia differences is seen in RRRobot also, but RRRobot's full dynamics is more complex because of the coupling between body pitch and yaw oscillations. We have earlier shown (Balasubramanian et al. 2006) that combining the decoupled models in Figure 11 provides a good approximation to the RRRobot's original fully integrated dynamics. We now present gaits for legless locomotion that use leg motions to exploit the interplay of pitch and yaw rotations and the contact constraints.

While many candidate leg motions, such as aperiodic and non-smooth trajectories, exist, we limit our analysis to sinusoidal leg trajectories for simplicity. We choose leg trajectories of the form $a \sin(\omega t + \beta) + \gamma$, where a represents the leg amplitude, ω the leg angular frequency, β the leg phase difference, and γ the leg offset. In this paper, we mainly study the influence of leg offset and leg phase difference on RRRobot's translation, while keeping the leg amplitude and frequency fixed. We choose leg oscillation amplitudes that keep body oscillation amplitudes small to minimize body–ground contact slip. We set leg oscillation frequency slightly greater than the natural oscillatory frequency to excite attitude oscillations of sufficient amplitude. We avoid high- and low-frequency leg oscillations, since the body motions induced by such leg motions do not exhibit the slip-free rocking and rolling behavior we are interested in exploring. In all our experiments, the robot starts from rest at the origin with the legs in the vertical position, and a proportional-derivative controller tracks the desired leg trajectories. The robot has no feedback about its global position and orientation, and thus runs "open loop".

4.1. Demonstrating Legless Locomotion using Experiments and Simulation

We begin with experiments to explore the influence of varying the leg offsets on RRRobot's planar translation, while keeping leg frequencies, leg phase difference, and leg amplitude fixed. We explore both individual gaits and gait transitions. We keep body oscillations small in order to minimize body–ground slip. This is required for proper comparison with the simulation results, which assume slip-free body–ground contact.

We use the following parameter values: servo mass $M_s = 0.053$ kg, leg reaction masses $M_l = 0.057$ kg, leg length $l = 0.1$ m, and gravity $g = 9.81$ m/s. Note that RRRobot's motion is particularly sensitive to mass distribution differences and ground traction, since RRRobot's motion relies on slip-free contact and small inertia differences arising from leg swing motions. We ensure that pitch oscillations and body–ground slip do not overwhelm these properties. The prototype

robot has a suspended tether providing servo power and control signals. With only the servos hinged on the body, we can control the untethered RRRobot mass distribution carefully, but must ensure that the disturbances from the tether are small. The tethered RRRobot's shell radius is 0.12 m, and battery and processor are modeled with weights $M_b = 0.3$ kg.

4.1.1. RRRobot's Linear and Curved Translation Gaits

In this section, we explore RRRobot's linear and curved translation gaits individually using simulations and experiments with the tethered RRRobot. We explore two specific versions of the sinusoidal gait: in Gait 1, the legs oscillate about the vertical position (offset $\pi/2$), and in Gait 2, the legs oscillate about a position $\pi/4$ off the horizontal in Gait 2. The leg amplitude is set to 0.3 rad and leg angular frequency to 7.5 rad/s. The experiments and simulations run for 100 s, and an overhead camera tracks the robot–ground contact-point's motion.

Gait 1 produces translation along the Y-axis (see Figure 12 and Extensions 4 and 5) by inducing body pitch–yaw oscillations and negligible body roll rotations. The robot translates at about 2.5 mm/s in the experiment and about 8 mm/s in the simulation.

Gait 2 produces counter-clockwise circular translation (see Figure 13 and Extensions 6 and 7) due to a combination of pitch–yaw oscillations, yaw drift (over time), and small roll oscillations. The robot covers half a circle in the experiment and the simulation, translating at about 2.5 mm/s and turning at about 1.5°/s. In both gaits, swapping the relative phase between the two legs produces translation in the opposite direction. The initial transients produced by ramping the legs from rest into the desired trajectories are visible in the experiment and the simulation, and dampen out after a few cycles.

Our experience indicates that gaits with leg offset close to the horizontal $(0, \pi)$ offer limited translation capability. This is because as the leg offset gets closer to the horizontal, pitch oscillations become smaller and roll oscillation amplitudes are too small to overcome ground friction losses. We thus focus on gaits with offset between $\pi/4$ and $3\pi/4$ (45° either side of the vertical).

The robot's paths produced in the simulation and the experiment match qualitatively. In particular, the path curvature in the simulation and the experiment match well—the robot translates linearly (curvature zero) in Gait 1, while it curves with radius approximately 0.1 m in Gait 2. While the robot's translation velocity in Gait 2 compares well between experiment and simulation, the robot's translation velocity in Gait 1 is smaller in the experiment than in the simulation and the difference in distance traveled builds up over time. The difference in Gait 1's translation velocity between the experiment and the simulation is probably due to errors in modeling ground friction. In particular, we believe that losses due to dry (static) friction in the experiment are larger in Gait 1 due to the jerky

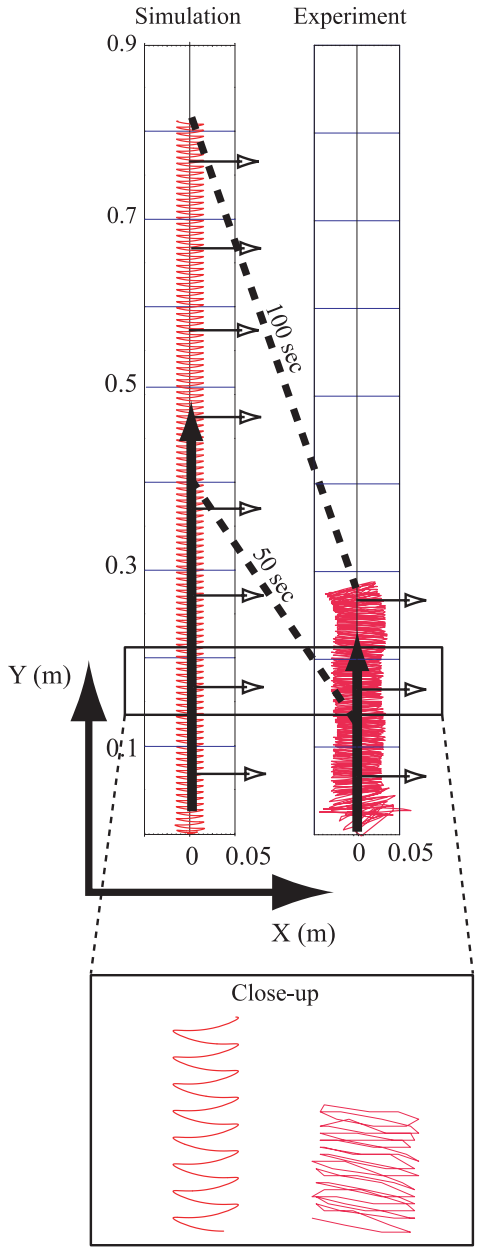

Fig. 12. Planar plots of contact-point time history during sideways locomotion produced by Gait 1 in RRRobot-on-a-plane simulation and RRRobot-on-a-plane experiment. The solid arrow gives robot motion direction, the dotted lines indicate the robot position at the specified time, and the white-headed arrows indicate robot yaw orientation. The close-up indicates how the paths match over a few cycles.

to and fro pitch–yaw oscillations. In contrast, Gait 2 induces simultaneous roll, pitch, and yaw oscillations, causing dry (static) friction effects to be reduced. Since dry friction effects are not modeled in the simulation, the robot's velocity using Gait 1

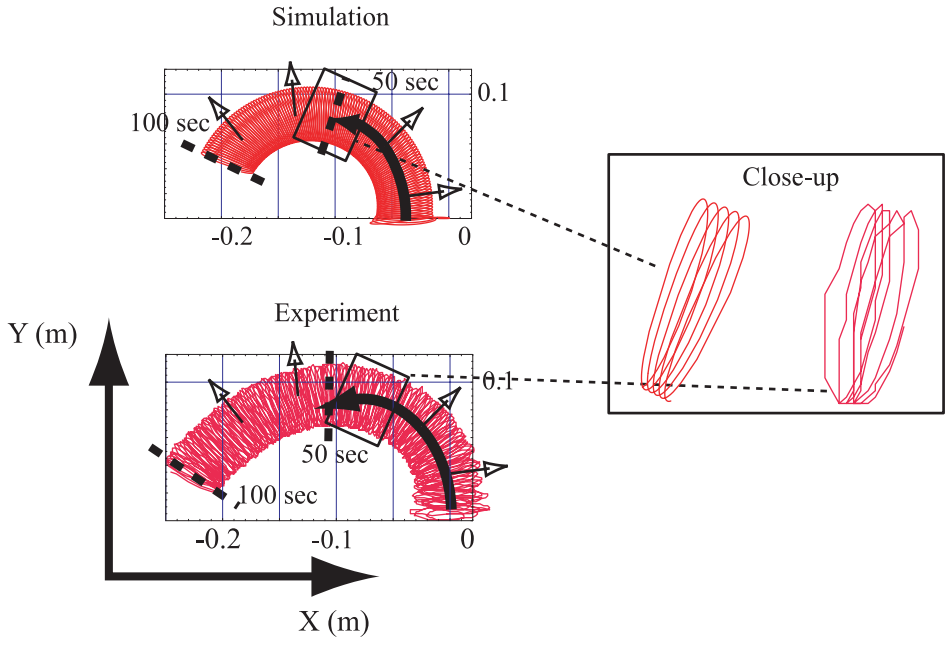

Fig. 13. Planar plots of contact-point time history during counter-clockwise circular locomotion produced by Gait 2 in the simulation and the experiment. The solid arrow gives robot motion direction, the dotted lines indicate the robot position at the specified time, and the white-headed arrows indicate robot yaw orientation. The close-up indicates how the paths match over a few cycles.

in the experiment is slower when compared with its velocity in the simulation. Our simulations of a tethered RRRobot bundle all ground-friction losses into the viscous damping coefficients by setting viscous damping ζ_{rr} to

$$\zeta_{rr} = (-0.6\dot{x}, -0.6\dot{y}, -0.05\dot{\theta}_r, -0.01\dot{\theta}_p, -0.0045\dot{\theta}_y, -0.01\dot{\phi}_1, -0.01\dot{\phi}_2)^{\mathrm{T}}. \quad (7)$$

Since legless locomotion is a dynamically coupled locomotion mode where the dynamic effect of the leg swings is transferred through the contact geometry to produce motion, the losses are larger and more difficult to model when compared with a conventional locomotion mode such as walking (see Section 4.1 for a discussion on modeling RRRobot's contact dynamics). In this paper, the models are intended to capture the structural quality, and not the complete quantitative details, of legless locomotion to permit approximate planning of translation when a robot is high-centered. In summary, legless locomotion offers an alternative locomotion mode, albeit incremental and approximate, when a robot is high-centered.

4.1.2. RRRobot Gait Transitions

While we presented an individual analysis of RRRobot's linear and curved translation gaits in the previous section, we now present an analysis of RRRobot's behavior when its gaits are sequenced. In particular, we use computer simulations and experiments with an untethered RRRobot to study how leg trajectory transients affect RRRobot's translation when changing from a linear translation gait to a curved translation gait and *vice versa*.

The untethered RRRobot is autonomous with the controller and power supply on-board, thus eliminating disturbances from the tether. The untethered RRRobot's mass distribution must be carefully tuned using weights to ensure symmetry, since the processor and battery weight is fixed to the hemisphere bottom. The untethered RRRobot's radius is 0.15 m, and battery and processor mass is $M_{\mathrm{b}} = 0.168$ kg.

We use sinusoidal leg trajectories (amplitude 0.65 rad, phase difference $\pi/2$, and frequency 7.5 rad/s) with the following sequence of leg offsets (see Figure 14(a) and (b)): leg offset $\pi/2$ for 80 cycles (period 1, linear translation expected), leg offset $5\pi/8$ for 40 cycles (period 2, curved translation expected), leg offset $\pi/2$ for 80 cycles (period 3, linear translation expected), and leg offset $3\pi/4$ for 40 cycles (period 4, curved translation expected). Smooth transitions from one gait to another are executed inside ten cycles. A Vicon motion-capture system[2] tracks the motion of the robot body (six markers on the hemisphere rim) and the legs (two markers on each leg) at 120 frames/s. The motion-capture data permits us to

2. See http://www.vicon.com.

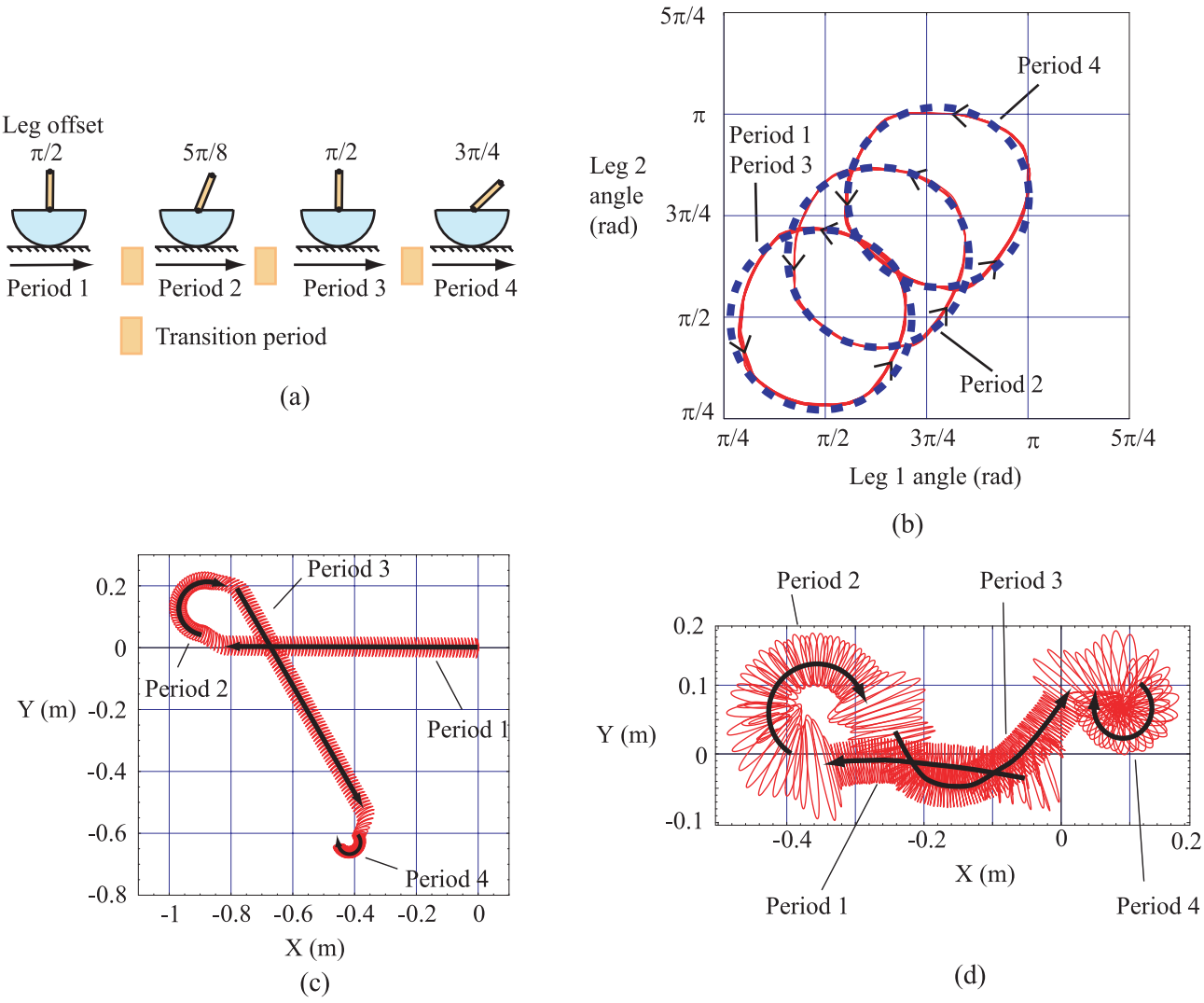

Fig. 14. The untethered RRRobot experiment and simulation. (a) Studying gait transitions in legless locomotion: the offset of the sinusoidal gaits change from $\pi/2$ to $5\pi/8$ to $\pi/2$ and then to $3\pi/4$. (b) Untethered RRRobot experiment: phase relationship between leg motions (red solid lines) during each period. The blue dotted lines indicate the desired trajectories. (c) RRRobot simulation: planar translation. (d) Untethered RRRobot experiment: planar translation.

perform a complete geometric analysis of RRRobot's motion. In reviewing the experiment and simulation results, we first examine the robot's translation, followed by the phase relationships between body rotations and leg motion, and finally how body rotations evolve over time.

Figure 14(c) shows the time history of planar translation in the simulation, and Figure 14(d) shows the time history of planar translation in the experiment (see Extension 8 for an animation created from motion capture). Since RRRobot runs open-loop, the robot drifts from the expected path in the experiment due to unmodeled disturbances and transients. This is seen particularly in the periods where the robot is supposed to translate linearly (periods 1 and 3). It would be interesting to find advanced feedback controllers that eliminate such drift to "close the loop". While examples of feedback controllers that combine dynamics and kinematics for wheeled robots exist (Fierro and Lewis 1998; Wilson and Robinett 2001; Zhu et al. 2006), finding feedback controllers for dynamic mobile robots with spherical kinematics remains an unsolved problem.

The robot's planar path in the experiment and the simulation match qualitatively. However, we again notice that RRRobot's linear translation velocity is slower in the experiment when compared with the simulation. We attribute this to the errors in ground traction modeling (see Section 3 for a discussion of contact modeling for legless locomotion). We also notice that the transients dampen out more quickly in the sim-

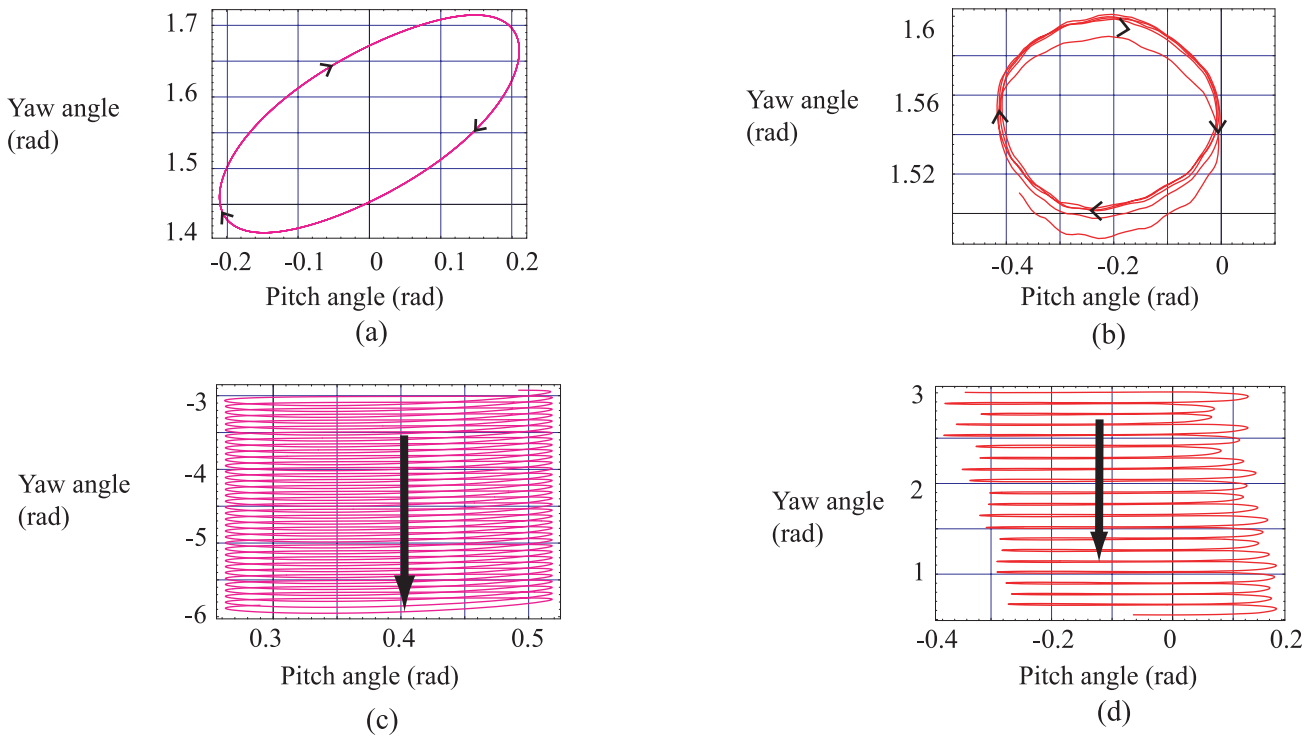

Fig. 15. The untethered RRRobot experiment and simulation. (a) RRRobot simulation: yaw–pitch phase relationship during period 1, (b) Untethered RRRobot experiment: yaw–pitch phase relationship during period 1, (c) RRRobot simulation: yaw–pitch phase relationship during period 4. (d) Untethered RRRobot experiment: yaw–pitch phase relationship during period 4.

ulation than in the experiment. The important point from Figures 14(c) and 14(d) is that RRRobot can translate approximately with variable curvature and has complete planar accessibility using different leg trajectory offsets. In addition to measuring RRRobot's planar translation, the motion capture data allows us to quantify RRRobot's body rotations and leg motions seen in our experiments and simulations. Figure 14(b) shows the phase relationship of the actual leg trajectories during each of the periods. We note two discrepancies in the leg trajectories. First, the leg angles are offset by about 8° (average across three periods) from the desired offset values. The inertias on the prototype robot had to be carefully balanced to ensure that the body pitch angle was zero, and so the leg trajectory offsets were modified slightly to ensure that the robot pitch was zero at the start. Second, while we expect to see circles because the commanded leg trajectories are $\pi/2$ out-of-phase with each other, the distorted circles indicate that there are errors in tracking the commanded leg trajectories. However, despite these errors, RRRobot's translation in the experiment is still predictable from the simulation, since legless locomotion has smoothly varying dynamics.

Figures 15(a) and 15(c) show the relationship between RRRobot's pitch and yaw rotations during period 1 and period 4 in the simulation, while Figures 15(b) and 15(d) show the relationship between RRRobot's pitch and yaw rotations during the same periods in the experiment. We note three interesting features.

First, we note that pitch and yaw are out-of-phase with each other in period 1, as evidenced by the non-zero area under the curve. As presented in Section 3.2, such out-of-phase attitude oscillations when coupled with the non-holonomic contact constraints produce net translation; this compares well with the linear translation induced by pitch–yaw oscillations in Figure 7.

Second, we note that yaw drifts in time during period 4, due to the out-of-phase leg oscillations offset from the vertical. Yaw drift combined with pitch–yaw oscillations induces RRRobot's translation to curve. This compares well with the example seen in Figure 10 where yaw drift causes the robot to translate in a circle.

Third, we note that the pitch–yaw rotations are not identical in the simulation and the experiment due to modeling errors. In the simulation, the yaw oscillation amplitude is bigger; also the pitch–yaw phase relationship is closer to $\pi/2$ in the experiment than in the simulation.

Figure 16(a) shows the time history of pitch rotations in the simulation, and Figure 16(b) the time history of pitch rotations in the experiment. In both experiment and simulation, the

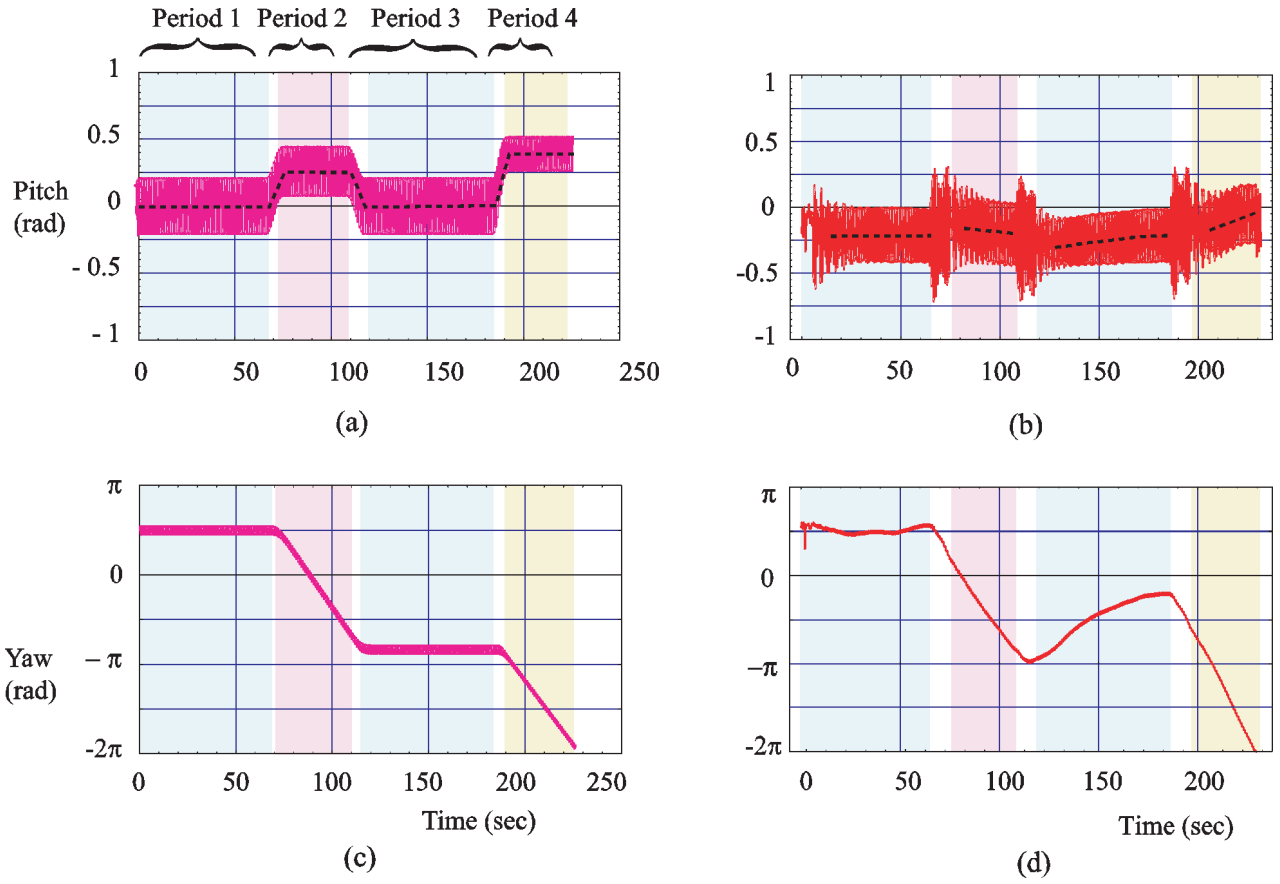

Fig. 16. The untethered RRRobot experiment and simulation. (a) RRRobot simulation: time history of pitch oscillations. (b) Untethered RRRobot experiment: time history of pitch oscillations. (c) RRRobot simulation: time history of yaw oscillations. (d) Untethered RRRobot experiment: time history of yaw oscillations.

mean pitch during periods 2 and 4 are different from those in periods 1 and 3, since the leg offsets are different and gravity causes the robot to lean (pitch) in the offset direction. However, while the mean pitch during periods 1 and 3 is zero in the simulation, pitch is offset from the vertical in the experiment due to small leg position and mass distribution errors in RRRobot. This causes RRRobot to translate along a curve during periods 1 and 3 in the experiment, rather than along a straight line. Also, pitch offset transients take longer to dampen out in the experiment than in the simulation. For example, the transients during period 3 dampen out slowly in the experiment, causing pitch oscillations to slowly settle into the limit cycle. This causes the translation path to curve during period 3 before settling into a linear translation path.

There is a strong similarity in RRRobot's yaw oscillations between the experiment and the simulation, except during period 3 when pitch transients take a long time to settle (see Figures 16(c) and (d)). RRRobot translates linearly during period 1 and curves during periods 2 and 4. Simply put, RRRobot's translation curves in the direction the robot pitches toward.

Finally, Figure 17 shows the time history of body roll rotations in the experiment. Note that the roll oscillation amplitudes are significantly smaller than the pitch oscillation amplitudes and have small impact on RRRobot's translation direction.

We also scanned RRRobot's body curvature to see if the plastic hemisphere deforms with the weight, since body deformations near the contact point influence the contact kinematics. In the nominal operating configuration (concave up), the hemisphere radius is 0.156 m, whereas the hemisphere in an inverted configuration (convex up) has radius 0.162 m (we fit a sphere to a set of points using the algorithm developed by Chang and Pollard (2006)). Note that we assume that the sphere radius is 0.15 m in our simulations. Despite the discrepancies in robot radius, the planar paths traversed in the simulation and the experiment qualitatively match.

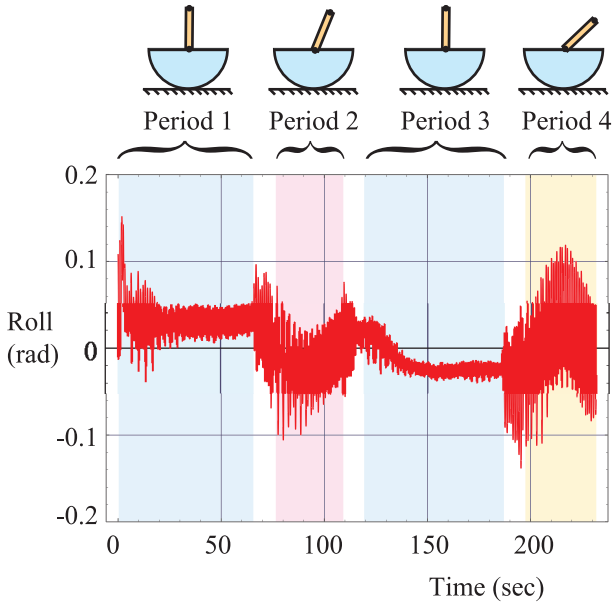

Fig. 17. Untethered RRRobot experiment: body roll oscillations.

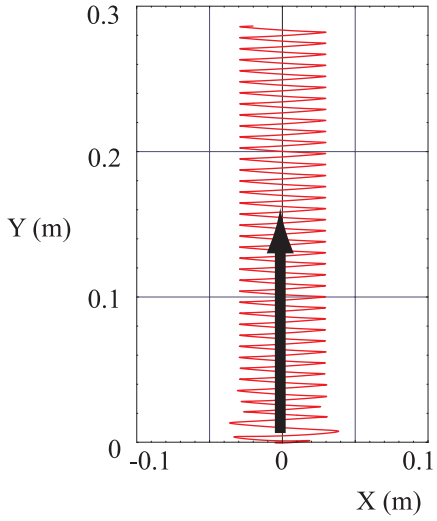

Fig. 18. RRRobot simulation: time history of contact-point motion induced by out-of-phase leg motions about the vertical configuration over 30 s.

Our simulations of an untethered RRRobot model ground traction by setting viscous damping ζ_{rr} to

$$\zeta_{rr} = (-2.0\dot{x}, -2.0\dot{y}, -0.01\dot{\theta}_r, -0.01\dot{\theta}_p, -0.004\dot{\theta}_y, -0.01\dot{\phi}_1, -0.01\dot{\phi}_2)^{\mathrm{T}}. \quad (8)$$

Note that these damping parameters are different from those used in simulating the smaller radius RRRobot (as discussed in the previous Section 4.1.1), since the ground traction losses differ between the two cases. Again, note that the translation and rolling damping coefficients are coupled, and more work is required to find the exact mapping between the losses in different freedoms. In this paper, the damping coefficients only approximate the ground traction forces seen in the experiment to find a qualitative agreement between the robot's translation in the experiment and the simulation.

Finally, note that the large ground friction forces in the experiment (and modeled using viscous damping in the simulation) cause RRRobot to move slowly. In the following section, we present simulation results with lesser viscous damping to model slip-free body–ground contact. As expected, this allows RRRobot to translate faster.

4.2. Exploring Legless Locomotion Capabilities using Simulation

In this section, we explore using simulation the full range of motions available to RRRobot by varying its leg trajectories. We use the following parameter values: servo mass $M_s = 0.053$ kg, leg reaction masses $M_l = 0.057$ kg, battery and processor mass $M_b = 0.3$ kg, sphere radius $r = 0.12$ m, leg length $l = 0.1$ m, and gravity $g = 9.81$ m/s. We use leg amplitude 0.3 rad and leg frequency 8 rad/s and set viscous damping to

$$\zeta_{rr} = (0, 0, -0.01\dot{\theta}_r, -0.01\dot{\theta}_p, -0.01\dot{\theta}_y, -0.01\dot{\phi}_1, -0.01\dot{\phi}_2)^{\mathrm{T}}. \quad (9)$$

Note that these damping coefficients are different from those we use to match experimental results in Section 4.1. The damping coefficients used in the previous section try to model the dry friction from body–ground slip and the viscous damping from the ground interaction, while from this section onwards we assume slip-free body–ground contact and only model the viscous damping.

Figure 18 shows RRRobot's translation induced by $\pi/2$ out-of-phase leg motions about the vertical configuration (simulation duration 25 s), while Figure 19 shows RRRobot's translation induced by $\pi/2$ out-of-phase leg motions offset $\pi/4$ from the vertical configuration (simulation duration 25 s). Note that the translation velocity is lesser in the curved translation gait. This is because the robot pitches, yaws, and rolls simultaneously, causing the contact point to trace loops in the plane. In contrast, RRRobot's body only pitches and yaws in the linear translation gait and does not trace loops.

Figure 20 shows how RRRobot's planar translation changes with varying leg offset and phase difference, based on RRRobot simulations using leg amplitude 0.3 rad and leg frequency 8 rad/s (simulation duration 100 s). Note that translation curvature depends predominantly on leg offset, and RRRobot curves

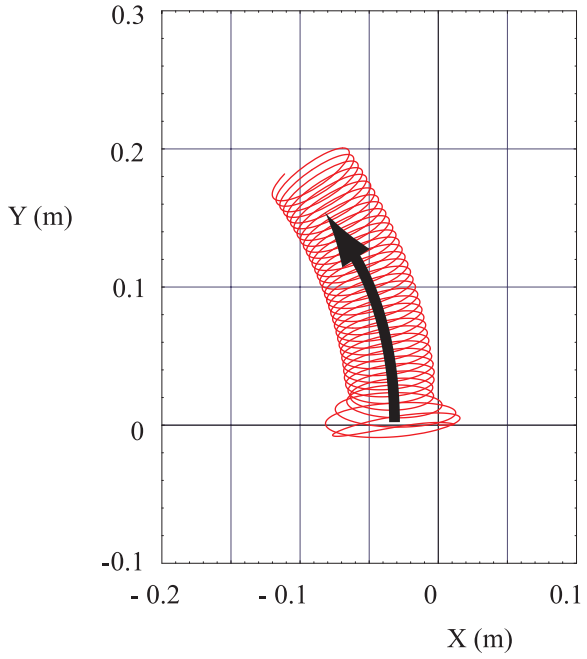

Fig. 19. RRRobot simulation: time history of contact-point motion induced by out-of-phase leg motions offset $\pi/4$ from the vertical configuration over 30 s.

in the direction it leans (pitches) in. For example, the robot curves to the left with leg offset $\pi/4$ and curves to the right with leg offset $3\pi/4$. Also, translation curvature is symmetric as leg offset varies either side of the vertical configuration. Thus, the simulations indicate, like the experiments, that translation with variable curvature is possible. This compares well with the intuition offered by the contact kinematics analysis in Section 3.2, where we showed that pitch–yaw oscillations induce lateral translation and such oscillations when combined with yaw drift induce curved motion. This is exactly what we see in RRRobot's dynamic motion—out-of-phase leg motions about the vertical produce pitch–yaw oscillations which induce RRRobot to translate along its body-fixed Y-axis; when RRRobot's leg offset shifts from the vertical, RRRobot's yaw drifts with time and induces curved translation.

Translation velocity varies depending on both leg offset and phase difference. Gauging from the path lengths in Figure 20, we notice that translation velocity is maximum (1 cm/s) with leg offset $\pi/2$ and phase difference $\pi/2$, since this induces large body pitch–yaw oscillations with body pitch–yaw phase difference close to $\pi/2$.

Figure 21 analyzes RRRobot's steady-state body rotations as a function of leg offset and phase difference. Notice that roll oscillation amplitudes are much smaller than pitch oscillation amplitudes, and this matches our intuition that RRRobot's translation is primarily due to out-of-phase pitch and yaw oscillations. RRRobot's pitch and yaw oscillation amplitudes do not vary much with leg offset, but change significantly with leg phase difference—as leg phase difference approaches zero, pitch oscillation amplitude increases and yaw oscillation amplitude decreases; as leg phase difference approaches π, pitch oscillation amplitude decreases and yaw oscillation amplitude increases. This observation matches with the intuition offered by the decoupled pitch and yaw dynamics models in Figure 11. Thus, there is a trade-off between pitch and yaw oscillation amplitudes as leg phase difference varies between $\pi/4$ and $3\pi/4$. The phase difference between yaw and pitch oscillations varies little from $\pi/2$ (see Figure 21(d)). We noticed in Section 3.2 that this pitch–yaw phase difference produces maximum translation velocity. So this choice of parameters, namely RRRobot's body masses, leg masses, and body curvature, induce RRRobot to translate with maximum linear velocity naturally.

4.3. Summary of RRRobot Experiments and Simulations

In this section, we have explored legless locomotion through both experimental studies and simulation. Using sinusoidal leg trajectories that induce variable-curvature translation, we have shown that RRRobot has full planar accessibility, albeit slow and approximate. The simulation and the experiment results match qualitatively, with the main difference being the slower linear translation velocity observed in the experiments as compared with the simulation. We believe this is the result of unmodeled body–ground dry friction.

5. Conclusion

Legless locomotion is a novel locomotion mode that is applicable in the special case where a robot is high-centered. The gaits we present show that translation is feasible, albeit slow and approximate, and the robot can travel anywhere in the plane. There may be many more novel locomotion strategies available to a robot when its conventional locomotory mode fails. Finding and understanding these different locomotion modes will contribute to improving a robot's robustness.

Unique from all previously studied locomotion, legless locomotion is continuous, oscillatory, and underactuated in the presence of gravity, variable inertia, and non-holonomic contact constraints. At this time, it is unclear how to apply previously used techniques in geometric control theory to study legless locomotion. Using experiment, simulation, and dynamics theory, we have provided a strong understanding of how legless locomotion works. Several interesting aspects of legless locomotion remain to be explored. For example, while we have used specific masses, spherical shells, and leg trajectories to illustrate legless locomotion's properties, it would be interesting to explore a dimensionless parametrization of legless locomotion. Also, more work is required to study the stability of legless locomotion's dynamics and to find a planning technique for legless locomotion's approximate translation.

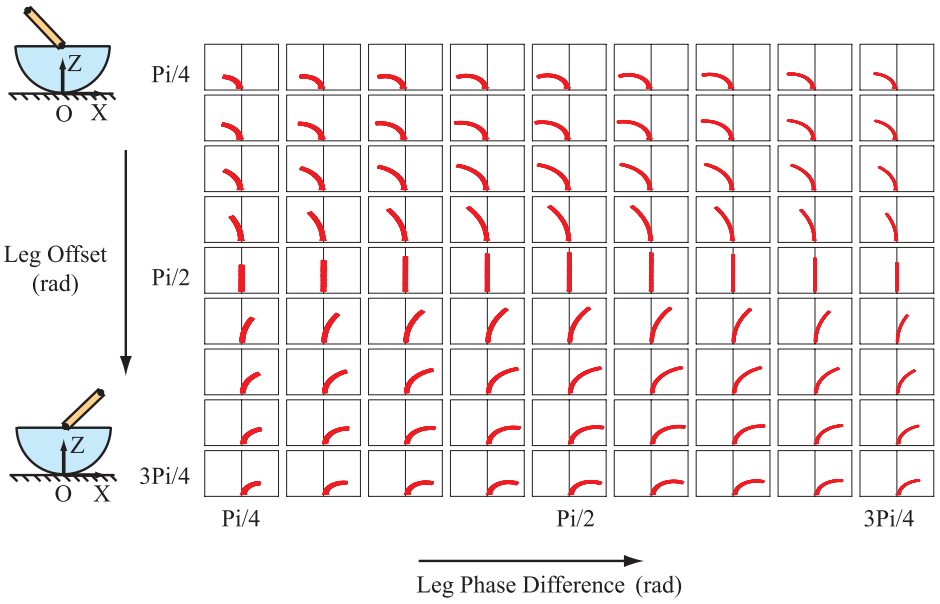

Fig. 20. Translation curvature as a function of leg trajectory offset and phase difference: each plot shows the time history of contact-point motion over 100 s. The X-axis range is $[-0.6, 0.6]$ m, and the Y-axis range is $[0, 1.1]$ m.

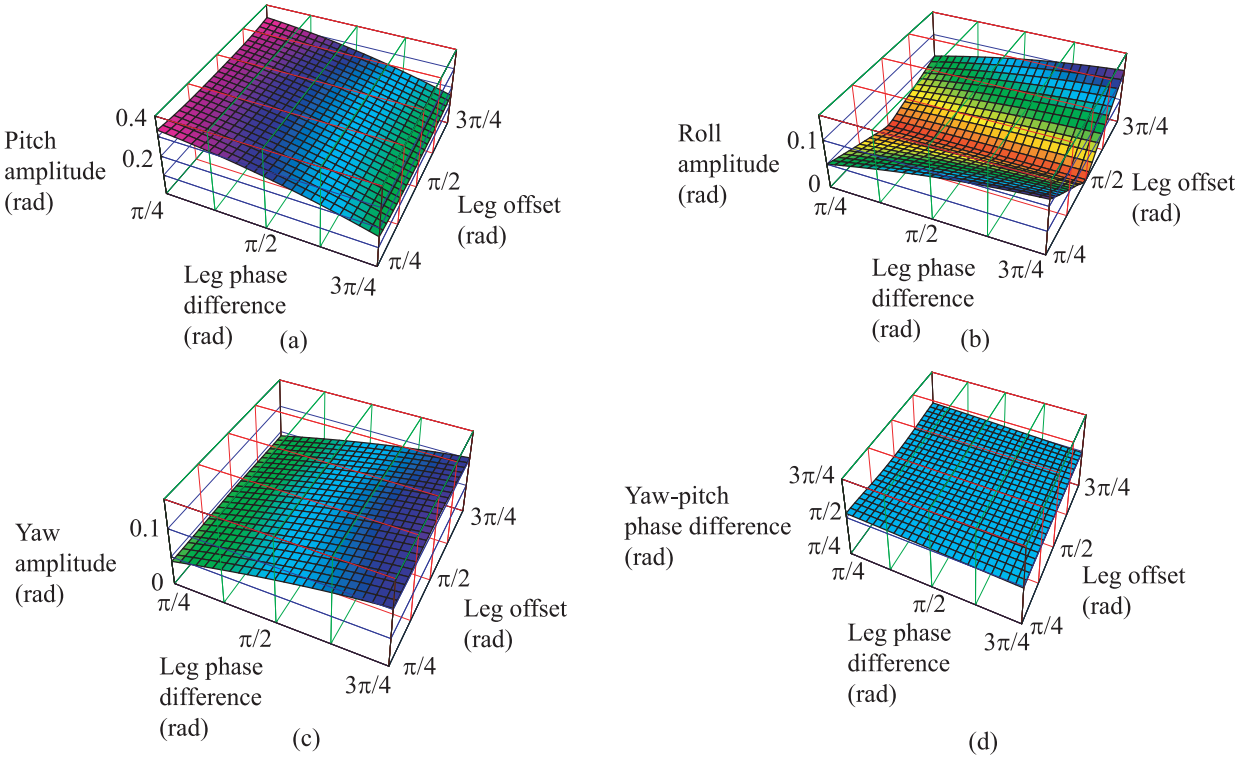

Fig. 21. The mapping between leg motions (offset and phase difference) and body oscillations: influence of leg motions on (a) pitch oscillation amplitude, (b) roll oscillation amplitude, (c) yaw oscillation amplitude, and (a) yaw–pitch oscillation phase difference.

Acknowledgments

The authors thank their colleagues from the Robotics Institute at Carnegie Mellon University for providing feedback in this research. In particular, we thank Brendan Meeder, Devin Balkcom, Elie Shammas, and Klaus Schmidt. This work was supported by NSF grant IIS 0082339, IIS 0222875, and DARPA/ONR N00014-98-1-0747 and was done at the Robotics Institute at Carnegie Mellon University.

Appendix: Index to Multimedia Extensions

The multimedia extension page is found at http://www.ijrr.org.

Table of Multimedia Extensions

Extension	Type	Description
1	Video	RHex escapes after becoming high-centered.
2	Video	A round-bottomed RHex locomotes by swinging its legs.
3	Video	A simulation of the sphere–plane contact kinematics illustrates a sphere can translate in any direction using roll, pitch, and yaw oscillations.
4	Video	Experiment showing RRRobot locomoting sideways.
5	Video	Simulation showing RRRobot locomoting sideways.
6	Video	Experiment showing RRRobot locomoting in a counter-clockwise path.
7	Video	Simulation showing RRRobot locomoting in a counter-clockwise path.
8	Video	Animation of experiment motion capture showing legless locomotion gait transitions.

References

Balasubramanian, R. (2006). Modeling and control techniques for a class of mobile robot error recovery problems. *Ph.D. Thesis*, Robotics Institute, Carnegie Mellon University.

Balasubramanian, R. and Rizzi, A. A. (2004). Kinematic reduction and planning using symmetry for a variable inertia mechanical system. *Proceedings of the IEEE/RSJ International Conference on Intelligent Robots and Systems*, Vol. 4, pp. 3829–3834.

Balasubramanian, R., Rizzi, A. A. and Mason, M. T. (2003). Legless locomotion for legged robots. *Proceedings of the International Conference on Robots and Intelligent Systems*, Vol. 1, pp. 880–885.

Balasubramanian, R., Rizzi, A. A. and Mason, M. T. (2004). Legless locomotion: Models and experimental demonstration. *Proceedings of the IEEE International Conference on Robotics and Automation*.

Balasubramanian, R., Rizzi, A. A. and Mason, M. T. (2006). Toward legless locomotion control. *Proceedings of the IEEE/RSJ International Conference on Intelligent Robots and Systems*.

Bares, J. and Wettergreen, D. (1999). Dante II: technical description, results and lessons learned. *International Journal of Robotics Research*, **18**(7): 621–649.

Bellaiche, A., Laumond, J., and Jacobs, P. (1991). Controllability of car-like robots and complexity of the motion planning problem. *Proceedings of the International Symposium on Intelligent Robotics*, pp. 322–337.

Berkemeier, M. D. and Fearing, R. S. (1998). Sliding and hopping gaits for the underactuated acrobot. *IEEE Transactions on Robotics and Automation*, **14**(4): 629–634.

Bhattacharya, S. and Agrawal, S. K.(2000). Spherical rolling robot: A design and motion planning studies. *IEEE Transactions on Robotics and Automation*, **16**(6): 835–839.

Bicchi, A., Balluchi, A., Prattichizzo, D. and Gorelli, A. (1997). Introducing the sphericle: an experimental testbed for research and teaching in nonholonomy. *Proceedings of the IEEE International Conference on Robotics and Automation*, pp. 2620–2625.

Bicchi, A. and Marigo, A. (2002). Dexterous grippers: Putting nonholonomy to work for fine manipulation, nonholonomy on purpose. *International Journal of Robotics Research*, **21**: 427–442.

Bloch, A., Baillieul, J., Crouch, P. and Marsden, J. (2003). *Nonholonomic Mechanics and Control*. Berlin, Springer.

Brilliantov, N. V. and Poschel, T. (1998). Rolling friction of a viscous sphere on a hard plane. *Europhysics Letters*, **42**: 511–516.

Bullo, F. and Lewis, A. D. (2003). Kinematic controllability and motion planning for the snakeboard. *IEEE Transactions on Robotics and Automation*, **19**(3): 494–498.

Camicia, C., Conticelli, F. and Bicchi, A. (2000). Nonholonomic kinematics and dynamics of the sphericle. *Proceedings of the IEEE International Conference on Intelligent Robots and Systems*, 805–810.

Carlson, J. and Murphy, R. R. (2005). How UGVs physically fail in the field. *IEEE Transactions on Robotics and Automation*, **21**(3): 423–437.

Chang, L. Y. and Pollard, N. S. (2006). Constrained least-squares optimization for robust estimation of center of rotation. *Journal of Biomechanics*, in press.

Craig, J. J. (1989). *Introduction to Robotics*. Reading, MA, Addison-Wesley.

Das, T. and Mukherjee, R. (2006). Reconfiguration of a rolling sphere: a problem in evolute-involute geometry. *Transac-*

tions of the ASME Journal of Applied Mechanics, **73**: 590–597.

Dowling, K. (1997). Limbless locomotion: learning to crawl with a snake robot. *Ph.D. Thesis*, Robotics Institute, Carnegie Mellon University.

Fernandes, C., Gurvits, L. and Li, Z. (1994). Near optimal nonholonomic motion planning for a system of coupled rigid bodies. *IEEE Transactions on Automatic Control*, **39**(3): 450–463.

Fierro, R. and Lewis, F. L. (1998). Control of a nonholonomic mobile robot using neural networks. *IEEE Transactions on Neural Networks*, **9**: 589–600.

Full, R. J. and Tu, M. S. (1991). Mechanics of a rapid running insect: Two-, four- and six-legged locomotion. *Journal of Experimental Biology*, **156**: 215–231.

Endo, G., Togawa, K. and Hirose, S. (1999). A self-contained and terrain-adaptive active cord mechanism. *Advanced Robotics*, **13**(3): 243–244.

Hale, E., Schars, N., Burdick, J. and Fiorini, P. (2000). A minimally actuated hopping robot for exploration of celestial bodies. *Proceedings of the IEEE International Conference On Robotics and Automation*.

Jean, F. (1996). The car with *n* trailers: characterization of the singular configurations. *ESAIM: COCV*, volume 1. http://www.emath.fr/cocv/.

Jose, J. V. and Saletan, E. J. (1998). *Classical Dynamics: A Contemporary Approach*. Cambridge, Cambridge University Press.

Krishnaprasad, P. S. and Tsakiris, D. P. (1998). Oscillations, SE(2)- snakes and motion control: a study of the roller racer. *Technical Report*, Institute for Systems Research, University of Maryland.

Laumond, J. (1998). *Robot Motion Planning and Control*. Berlin, Springer.

Lee, W. H. and Sanderson, A. C. (2002). Dynamic rolling locomotion and control of modular robots. *IEEE Transactions on Robotics and Automation*, **18**(1): 32–41.

Lewis, A., Ostrowski, J., Murray, R. and Burdick, J. (1994). Nonholonomic mechanics and locomotion: The snakeboard example. *Proceedings of the International Conference on Robotics and Automation*, Vol. 3, pp. 2391–2397.

Li, Z. and Canny, J. (1990). Motion of two rigid bodies with rolling constraint. *IEEE Transactions on Robotics and Automation*, **6**(1): 62–72.

Linnemann, R., Klaassen, B. and Kirchner, F. (2001). Walking robot scorpion—experiences with a full parametric model. *15th European Simulation Multiconference on Modeling and Simulation*, pp. 1012–1018.

Luca, F. and Risler, J.-J. (1994). The maximum of the degree of nonholonomy for the car with *n* trailers. *Proceedings of the IFAC Symposium on Robot Control*, pp. 165–170.

Lyons, D. and Pamnany, K. (2005). Rotational legged locomotion. *Proceedings of the International Conference on Advanced Robotics*, pp. 223–228.

McGeer, T. (1990). Passive dynamic walking. *International Journal of Robotics Research*, **18**(9): 917–930.

McMahon, T. A. (1984). Mechanics of locomotion. *The International Journal of Robotics Research*, **3**(2): 4–28.

Montana, D. J. (1988). The kinematics of contact and grasp. *The International Journal of Robotics Research*, **7**(3): 17–32.

Mukherjee, R., Minor, M. A. and Pukrushpan, J. (2002). Motion planning for a spherical mobile robot: Revisiting the classical ball-plate problem. *ASME Journal of Dynamic Systems Measurement and Control*, **124**(4): 502–511.

Murray, R. M., Li, Z. X. and Sastry, S. S. (1994). *A Mathematical Introduction to Robotic Manipulation*. Boca Raton, FL, CRC Press.

Nagasaka, K., Kuroki, Y., Suzuki, S., Itoh, Y. and Yamaguchi, J. (2004). Integrated motion control for walking, jumping and running on a small bipedal entertainment robot. *Proceedings of the 9th RSJ/JSME Robotics Symposia of Japan*, pp. 386–391.

Ostrowski, J. P. (1996). The mechanics and control of undulatory robotic locomotion. *Ph.D. Thesis*, California Institute of Technology.

Phipps, C. C. and Minor, M. A. (2005). Introducing the hexa-ball, a hybrid locomotion terrain adaptive walking and rolling robot. *Proceedings of the Climbing and Walking Robots*.

Poschel, T., Schwager, T. and Brilliantov, N. V. (1999). Rolling friction of a hard cylinder on a viscous plane. *The European Physical Journal B—Condensed Matter and Complex Systems*, **10**(1): 169–174.

Raibert, M. H. (1986). *Legged Robots that Balance*. Cambridge, MA, MIT Press.

Reeds, J. A. and Shepp, R. A. (1990). Optimal paths for a car that goes both forwards and backwards. *Pacific Journal of Mathematics*, **145**(2): 367–393.

Reznik, D. and Canny, J. (1998). A flat rigid plate is a universal planar manipulator. *Proceedings of the International Conference on Robotics and Animation*.

Rui, C., Kolmanovsky, I. V. and McClamroch, N. H. (2000). Nonlinear attitude and shape control of spacecraft with articulated appendages and reaction wheels. *IEEE Transactions on Automatic Control*, **45**(8): 1455–1469.

Sakagami, Y., Watanabe, R., Aoyama, C., Matsunaga, S., Higaki, N. and Fujimura, K. (2002). Intelligent asimo: System overview and integration. *Proceedings of the IEEE International Conference on Intelligent Robots and Systems*, pp. 2478–2483.

Saranli, U., Buehler, M. and Koditschek, D. E. (2001). RHex: A simple and highly mobile hexapod robot. *International Journal of Robotics Research*, **20**(7): 616–631.

Saranli, U. and Koditschek, D. (2002). Back flips with a hexapedal robot. *Proceedings of the IEEE International Conference On Robotics and Automation*, Vol. 3, pp. 2209–2215.

Shammas, E. A., Choset, H. and Rizzi, A. A. (2007). Towards a unified approach to motion planning for dynamic underactuated mechanical systems with non-holonomic constraints. *International Journal of Robotics Research*, **26**(10): 1075–1124.

Shores, B. and Minor, M. (2005). Design, kinematic analysis, and quasi-steady control of a morphic rolling disk biped climbing robot. *Proceedings of the IEEE International Conference on Robotics and Automation*.

Sofman, B., Lin, E., Bagnell, J., Cole, J., Vandapel, N. and Stentz, A. (2006). Improving robot navigation through self-supervised online learning. *Journal of Field Robotics* 23(12): 1059–1075.

Sussmann, H. and Tang, W. (1991). Shortest paths for the Reeds–Shepp car: a worked out example of the use of geometric techniques in nonlinear optimal control. *Technical Report SYCON-91-10*, Rutgers University.

Tunstel, E. (1999). Evolution of autonomous self-righting behaviors for articulated nanorovers. *Proceedings of the International Symposium on Artificial Intelligence, Robotics and Automation in Space (i-SAIRAS)*, pp. 341–346.

Verma, V., Gordon, G., and Simmons, R. (2003). Efficient monitoring for planetary rovers. *Proceedings of International Symposium on Artificial Intelligence, Robotics and Automation in Space*.

Wilson, D. G. and Robinett, D. R. III (2001). Robust adaptive backstepping control for a nonholonomic mobile robot. *Proceedings of the IEEE International Conference on Systems, Man and Cybernetics*, pp. 3241–3245.

Yamawaki, T., Mori, O. and Omata, T. (1994). Nonholonomic dynamic rolling control of reconfigurable 5r closed kinematic chain robot with passive joints. In *Proceedings of the IEEE International Conference on Robotics and Automation*, pp. 4054–4059.

Yim, M. (1994). New locomotion gaits. *Proceedings of the IEEE International Conference on Robotics and Automation*, pp. 2508–14.

Zeglin, G. (1999). The bow leg hopping robot. *Ph.D. Thesis*, Robotics Institute, Carnegie Mellon University.

Zenkov, D., Bloch, A. and Marsden, J. (1997). The energy-momentum method for the stability of nonholonomic systems. *Technical Report*, California Institute of Technology.

Zhu, X., Minor, M. A. and Park, S.-Y. (2006). Distributed robust control of compliant framed wheeled modular mobile robots. *ASME Journal of Dynamic Systems, Measurement, and Control*, **128**(3): pp489–498.